Title
Modular bimetallic complexes with a sulfonamido-based ligand

Journal
Dalton Transactions, 47(35)

ISSN
1477-9226

Authors
Lau, Nathanael
Sano, Yohei
Ziller, Joseph W
et al.

Publication Date
2018-09-11

DOI
10.1039/c8dt02455c

Peer reviewed

HHS Public Access

Author manuscript

Dalton Trans. Author manuscript; available in PMC 2019 September 11.

Published in final edited form as:

Dalton Trans. 2018 September 11; 47(35): 12362–12372. doi:10.1039/c8dt02455c.

Modular Bimetallic Complexes with a Sulfonamido-Based Ligand

Nathanael Lau[a], **Yohei Sano**, **Joseph W. Ziller**, and **A.S. Borovik**[*]

[a]Department of Chemistry, University of California – Irvine, 1102 Natural Sciences II, Irvine, CA 92697-2025, United States

Graphical Abstract

A series of modular unsymmetrical bimetallic complexes has been developed in which the key components can be easily substituted.

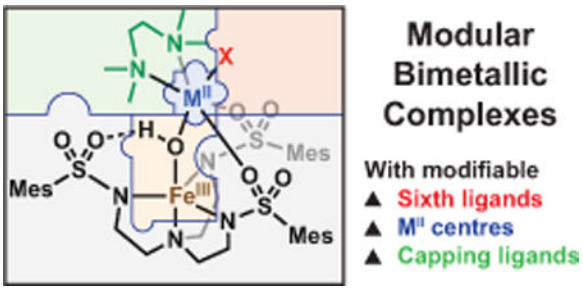

A series of bimetallic complexes prepared with the ligands *N,N,N′,N′*-tetramethylethane-1,2-diamine (TMEDA) and *N,N′,N″*-[2,2′,2″-nitrilotris(ethane-2,1-diyl)]tris(2,4,6-trimethylbenzenesulfonamido) ($[MST]^{3-}$) is described. Four diiron compounds of the formulation $(TMEDA)Fe^{II}(X)-(\mu\text{-}OH)-Fe^{III}MST$ were prepared, in which the X^- ligands are the anions OTf^-, Br^-, SCN^-, or N_3^-. Additionally, two heterobimetallic compounds of the formulation $(TMEDA)M^{II}(OTf)-(\mu\text{-}OH)-Fe^{III}MST$ (M^{II} = Co^{II} or Ni^{II}) were synthesized. All these compounds have similar spectroscopic and structural properties. All the diiron compounds exhibit perpendicular-mode electron paramagnetic resonance spectra consistent with S = 1/2 spin ground states, which is expected for high-spin Fe^{II} and Fe^{III} centres that are antiferromagnetically coupled. The heterobimetallic $(TMEDA)Ni^{II}(OTf)-(\mu\text{-}OH)-Fe^{III}MST$ complex had a spin states of S = 3/2 that also resulted from antiferromagnetic coupling between the high-spin Ni^{II} and Fe^{III} centres. The modularity of this system is further demonstrated by the substitution of the TMEDA ligand with ethylenediamine (en); for this species two equivalents of en coordinate to the Fe^{II} centre to form $[(en)_2Fe^{II}-(\mu\text{-}OH)-Fe^{III}MST]OTf$. These results demonstrate that a modular bimetallic system has been developed in which the key components can be modified.

aborovik@uci.edu.

‡See supporting information for crystallographic, UV-vis ,ESI-MS, and CV data for all complexes.

Introduction

Bimetallic complexes are key targets for many applications because of their desirable functional properties. For instance, the presence of two metal centres can facilitate cooperative multi-electron processes with first row transition metal ions that normally favour single-electron processes when reacted alone.[1,2] In catalysis, bimetallic units can provide different reaction pathways, faster reaction rates, and greater selectivity than their monometallic counterparts.[3–5] In addition, tuning the physical and chemical properties of bimetallic complexes is possible by independently modulating the structures of the two metal ions.[6]

Many ligands have been designed to promote formation of bimetallic complexes. For example, symmetrical dinucleating ligands have been designed to bind two metal centre with identical coordination environments.[7–14] Often, such ligands are treated with a single metal ion to prepare symmetrical homobimetallic complexes, but in some cases, heterobimetallic complexes can be prepared *via* the stepwise addition of different metal ions.[15–17]

It is synthetically more challenging to synthesize ligands that are capable of binding two metal centres with substantially different coordination environments, thus forming unsymmetrical bimetallic complexes. Some groups have designed “double-decker” ligands, which are dinucleating ligands with two different metal binding sites situated proximal to each other, and the close proximity of the metal centres often results in the formation of metal-metal bonds.[18–23] A different approach involves tethering two very different binding environments together to form unsymmetrical ligands, but this process often requires extensive ligand synthesis.[24–26]

Another approach involves preparing unsymmetrical bimetallic complexes by combining two different monometallic complexes.[27–33] This method often requires one monometallic fragment to have a ligand that is capable of interacting with a second metal centre, resulting in the formation of unsymmetrical bimetallic complexes. Because the systematic substitution of starting complexes provides for the preparation of modular bimetallic complexes, this method produces systems whose properties can be readily varied. We have has used this approach to prepare a series of unsymmetrical bimetallic compounds, using the tripodal ligand *N,N’,N”*-[2,2’,2”-nitrilotris(ethane-2,1-diyl)]tris(2,4,6-tri-methylbenzenesulfon-amido) ([MST]$^{3-}$) as the ligand scaffold.[34] This ligand was designed so that the sulfonamido O-atoms served as hydrogen bond (H-bond) acceptors within the secondary coordination sphere of a metal ion (Figure 1), and it has been used to prepare complexes with terminal hydroxido, aqua, or ammine ligands.[34,38–42] We also discovered that the sulfonamido O-atoms are able to interact with Lewis acids, most notably alkaline earth or transition metal ions. This feature allows for the preparation of discretely bimetallic complexes with the formulation [(L)M^{II}−(μ-OH)−M^{III}MST]$^{+}$ (Figure 1). A variety of different bimetallic complexes can be synthesized, including combinations of M^{II} = Ca^{II}, Sr^{II}, Ba^{II}, Mn^{II}, Fe^{II}, Co^{II}, Ni^{II}, Cu^{II}, Zn^{II} and M^{III} = Mn^{III}, Fe^{III}, Co^{III}, Ga^{III}, In^{III} ions.[34–38,43]

Our initial studies with these types of compounds involved the preparation of heterobimetallic complexes with redox inactive divalent metal ions (M^{II} = Ca^{II}, Sr^{II}, Ba^{II})

that were capped with crown ethers (L = 15-crown-5 or 18-crown-6, Figure 1A).[35] We subsequently reported on bimetallic complexes in which both metal centres were transition metal ions, using 1,4,7-trimethyl-1,4,7-triazacyclononane (TMTACN) to complete the primary coordination sphere of the M^{II} ion (Figure 1B).[36,37] All of these complexes had coordinatively saturated M^{II} centres because of the relatively high denticity capping ligands.

We have been exploring other types of ligands that are able to provide at least one substitution labile coordination site on the M^{II} centre that could facilitate the binding of an additional, external ligand. Toward this goal, we describe the preparation of a new bimetallic compound with the formulation [(TMEDA)Fe^{II}(OTf)−(μ-OH)−Fe^{III}MST] (denoted as [TMEDA-Fe^{II}(OTf)(OH)Fe^{III}], TMEDA is *N,N,N′,N′*-tetramethylethane-1,2-diamine, Figure 2). In this complex, the weakly coordinating OTf^- (triflate) anion can be displaced by other external ligands to produce a new series of diiron compounds. To further demonstrate synthetic versatility associated with this system, the analogous heterobimetallic complexes [TMEDA-M^{II}(OTf)(OH)Fe^{III}] (M^{II} = Co^{II}, Ni^{II}) were also prepared and characterized. Finally, we show that the TMEDA ligand can be substituted with the less hindered bidentate ligand ethylenediamine (en) to afford [$(en)_2Fe^{II}$−(μ-OH)−Fe^{III}MST]OTf, which has different structural properties.

Experimental section

General Methods

All reagents were purchased from commercial sources and used as received, unless otherwise noted. Solvents were sparged with argon and dried over columns containing Q-5 and molecular sieves. Potassium hydride (KH) as a dispersion in mineral oil was filtered with a medium porosity glass-fritted funnel and washed 5 times each with pentane and diethyl ether (Et_2O). Solid KH was dried under vacuum and stored under inert atmosphere. The synthesis of the ligand was carried out in the air and the preparations of the metal complexes were conducted in a Vacuum Atmospheres, Co. drybox under an argon atmosphere. Dioxygen was dried on a Drierite gas purifier purchased from Fischer Scientific. TMEDA and en were distilled over CaO and KOH under static vacuum at 30 °C onto 4 Å molecular sieves and stored under inert atmosphere. $Fe^{II}(OTf)_2{\cdot}2MeCN$,[44] $Co^{II}(OTf)_2{\cdot}2MeCN$,[44] $Ni^{II}(OTf)_2{\cdot}5MeCN$,[44] NMe_4[Fe^{II}MST],[35] NMe_4(SCN),[45] and $NMe_4(N_3)$[46] were synthesized according to previous reports.

Complex Synthesis

[TMEDA-Fe^{II}(OTf)(OH)Fe^{III}].—This compound was prepared by the literature procedure for the related salt [(TMTACN)Fe^{II}−(μ-OH)−Fe^{III}MST]OTf[36] using $Fe^{II}(OTf)_2{\cdot}$ 2MeCN (46.1 mg, 106 mmol), TMEDA (13.2 mg, 114 mmol), and NMe_4[Fe^{II}MST] (86.6 mg, 106 mmol) to produce the desired complex in crystalline yields of 62–87%. Crystals could be obtained *via* layering either THF or CH_2Cl_2 solutions of the salt with pentane. However, dark orange needle crystals of [TMEDA-Fe^{II}(OTf)(OH)Fe^{III}] suitable for X-ray diffraction were only grown from THF solutions layered under pentane. Elemental analysis calcd. for [TMEDA-Fe^{II}(OTf)Fe^{III}]·0.5CH_2Cl_2, $C_{40.5}H_{63}ClF_3Fe_2N_6O_{10}S_4$: C, 43.19; H, 5.64; N, 7.46%, found: C, 42.89; H, 5.34; N, 7.34%. UV-vis (CH_2Cl_2, λ_{max}, nm (ε_{max}, $M^{-1}cm^{-1}$))

274(sh), 283(sh), 380(6800). FTIR (ATR, cm^{-1}, selected bands): 3272(OH), 2980, 2935, 2869, 1603, 1564, 1467, 1313, 1276, 1239, 1129, 1034, 953, 816, 662, 635, 609. (Nujol, cm^{-1}): 3260(OH). Exact mass calcd for $[TMEDA\text{-}Fe^{II}(OH)Fe^{III}]^+$, $C_{39}H_{62}Fe_2N_6O_7S_3$: 934.3 found: 934.2. $E_{1/2}$ (MeCN, V versus $[FeCp_2]^{+/0}$): –0.84.

$[TMEDA\text{-}Fe^{II}(Br)(OH)Fe^{III}]$.—This compound was prepared using the method described above for $[TMEDA\text{-}Fe^{II}(OTf)(OH)Fe^{III}]$ with $Fe^{II}Br_2$ (20.5 mg, 0.0951 mmol), TMEDA (10.5 mg, 0.0902 mmol), and $NMe_4[Fe^{II}MST]$ (73.2 mg, 0.0893 mmol) to produce the desired complex in crystalline yields of 46–62%. Dark orange block crystals of $[TMEDA\text{-}Fe^{II}(Br)(OH)Fe^{III}]$ suitable for X-ray diffraction were grown from a CH_2Cl_2 solution layered under pentane. Elemental analysis calcd. for $[TMEDA\text{-}Fe^{II}(Br)(OH)Fe^{III}]\cdot 0.5CH_2Cl_2$, $C_{39.5}H_{63}ClBrFe_2N_6O_7S_3$: C, 44.63; H, 5.81; N, 7.97%, found: C, 44.88; H, 6.01; N, 7.95%. UV-vis (CH_2Cl_2, λ_{max}, nm (ε_{max}, $M^{-1}cm^{-1}$)) 276(sh), 284(sh), 386(6100). FTIR (ATR, cm^{-1}, selected bands): 3286(OH), 2981, 2933, 2893, 2865, 1602, 1562, 1464, 1277, 1126, 1071, 953, 935, 818, 660. (Nujol, cm^{-1}): 3288(OH). Exact mass calcd for $[TMEDA\text{-}Fe^{II}(OH)Fe^{III}]^+$, $C_{39}H_{62}Fe_2N_6O_7S_3$: 934.3 found: 934.1. $E_{1/2}$ (MeCN, V versus $[FeCp_2]^{+/0}$): –0.85.

$[TMEDA\text{-}Fe^{II}(NCS)(OH)Fe^{III}]$.—A solution of $[TMEDA\text{-}Fe^{II}(OTf)(OH)Fe^{III}]$ (88.0 mg, 0.0812 mmol) in tetrahydrofuran (THF) (10 mL) was treated with $NMe_4(SCN)$ (10.9 mg, 0.0824 mmol) and stirred. After 1 h volatiles were removed under reduced pressure to afford a solid, which was redissolved in CH_2Cl_2 and filtered through a medium porosity glass-fritted funnel to remove the insoluble $NMe_4(OTf)$. The filtrate was layered under pentane, and dark orange block crystals suitable for X-ray diffraction were obtained. The crystals were collected on a medium porosity glass-fritted funnel and dried under vacuum, resulting in crystalline product in yields of 58–78%. Elemental analysis calcd. for $[TMEDA\text{-}Fe^{II}(NCS)(OH)Fe^{III}]\cdot CH_2Cl_2$, $C_{41}H_{64}Cl_2Fe_2N_7O_7S_4$: C, 45.69; H, 5.99; N, 9.10%, found: C, 45.45; H, 6.04; N, 9.01%. UV-vis (CH_2Cl_2, λ_{max}, nm (ε_{max}, $M^{-1}cm^{-1}$)) 275(sh), 285(sh), 392(7000). FTIR (ATR, cm^{-1}, selected bands): 3278(OH), 2978, 2912, 2886, 2860, 2056(CN), 1603, 1564, 1470, 1456, 1350, 1259, 1102, 1031, 962, 817, 657, 638. (Nujol, cm^{-1}): 3271(OH), 2064(CN). Exact mass calcd for $[TMEDA\text{-}Fe^{II}(OH)Fe^{III}]^+$, $C_{39}H_{62}Fe_2N_6O_7S_3$: 934.3 found: 934.2. $E_{1/2}$ (MeCN, V versus $[FeCp_2]^{+/0}$): –0.89.

$[TMEDA\text{-}Fe^{II}(N_3)(OH)Fe^{III}]$.—This compound was prepared using the method described above for $[TMEDA\text{-}Fe^{II}(NCS)(OH)Fe^{III}]$ using $[TMEDA\text{-}Fe^{II}(OTf)(OH)Fe^{III}]$ (100. mg, 0.925 mmol) and $NMe_4(N_3)$ (11.1 mg, 0.955 mmol) to produce the desired complex as a crystalline solid in yields of 48–58%. Dark orange block crystals of $[TMEDA\text{-}Fe^{II}(N_3)(OH)Fe^{III}]$ suitable for X-ray diffraction were grown from a CH_2Cl_2 solution layered under pentane. Elemental analysis calcd. for $[TMEDA\text{-}Fe^{II}(N_3)(OH)Fe^{III}]\cdot CH_2Cl_2$, $C_{40}H_{64}Cl_2Fe_2N_9O_7S_3$: C, 45.25; H, 6.08; N, 11.87%, found: C, 45.55; H, 6.10; N, 12.15%. UV-vis (CH_2Cl_2, λ_{max}, nm (ε_{max}, $M^{-1}cm^{-1}$)) 275(sh), 285(sh), 389(6500). FTIR (ATR, cm^{-1}, selected bands): 3270(OH), 2913, 2938, 2909, 2863, 2842, 2069 (N_3), 1602, 1562, 1465, 1339, 1276, 1130, 1093, 1070, 1051, 1032, 952, 933, 850, 818, 661. (Nujol, cm^{-1}): 3271(OH), 2080(N_3). Exact mass calcd for $[TMEDA\text{-}Fe^{II}(OH)Fe^{III}]^+$, $C_{39}H_{62}Fe_2N_6O_7S_3$: 934.3 found: 934.2. E_c (MeCN, V versus $[FeCp_2]^{+/0}$): –0.99.

[TMEDA-Co^{II}(OTf)(OH)Fe^{III}].—This compound was prepared using the method described above for [TMEDA-Fe^{II}(OTf)(OH)Fe^{III}] using Co^{II}(OTf)$_2$·2MeCN (39.2 mg, 0.0895 mmol), TMEDA (10.9 mg, 0.0936 mmol), and NMe$_4$[Fe^{II}MST] (73.2 mg, 0.0893 mmol) to produce the desired complex as a crystalline solid in yields of 62–85%. Dark orange needle crystals of [TMEDA-Co^{II}(OTf)(OH)Fe^{III}] suitable for X-ray diffraction were grown from a THF solution layered under pentane. Elemental analysis calcd. for [TMEDA-Co^{II}(OTf)(OH)Fe^{III}] ·0.5C$_5$H$_{12}$, C$_{42.5}$H$_{68}$CoF$_3$FeN$_6$O$_{10}$S$_4$: C, 45.45; H, 6.10; N, 7.48%, found: C, 45.52; H, 5.96; N, 8.00%. UV-vis (CH$_2$Cl$_2$ solution λ_{max}/nm (ε_{max}/M^{-1}cm^{-1})) 275(sh), 387(4700). FTIR (ATR, cm^{-1}, selected bands): 3316(OH), 2975, 2935, 2871, 1603, 1467, 1311, 1278, 1239, 1220, 1129, 1073, 1037, 967, 953, 935, 851, 817, 662, 635, 609. (Nujol, cm^{-1}): 3312(OH). Exact mass calcd for [TMEDA-Co^{II}(OH)Fe^{III}]$^+$, C$_{39}$H$_{62}$FeCoN$_6$O$_7$S$_3$: 937.3 found: 937.1. $E_{1/2}$ (MeCN, V versus [FeCp$_2$]$^{+/0}$): –0.86. μ_{eff} (μ_B): 5.85.

[TMEDA-Ni^{II}(OTf)(OH)Fe^{III}].—This compound was prepared using the method described above for [TMEDA-Fe^{II}(OTf)(OH)Fe^{III}] using Ni^{II}(OTf)$_2$·5MeCN (50.2 mg, 0.0893 mmol), TMEDA (10.9 mg, 0.0936 mmol), and NMe$_4$[Fe^{II}MST] (73.6 mg, 0.0898 mmol) to produce the desired complex as a crystalline solid in yields of 60–67%. Dark orange block crystals of [TMEDA-Ni^{II}(OTf)(OH)Fe^{III}] suitable for X-ray diffraction were grown from a CH$_2$Cl$_2$ solution layered under pentane. Elemental analysis calcd. for [TMEDA-Ni^{II}(OTf)(OH)Fe^{III}] ·0.5C$_5$H$_{12}$, C$_{42.5}$H$_{68}$NiF$_3$FeN$_6$O$_{10}$S$_4$: C, 45.46; H, 6.10; N, 7.48%, found: C, 45.74; H, 5.59; N, 7.96%. UV-vis (CH$_2$Cl$_2$ solution λ_{max}/nm (ε_{max}/M^{-1}cm^{-1})) 275(sh), 285(sh), 382(6500). FTIR (ATR, cm^{-1}, selected bands): 3341(OH), 2974, 2935, 2871, 2361, 1603, 1308, 1242, 1221, 1130, 1073, 1044, 968, 954, 936, 817, 648. (Nujol, cm^{-1}): 3345(OH). Exact mass calcd for [TMEDA-Ni^{II}(OH)Fe^{III}]$^+$, C$_{39}$H$_{62}$FeNiN$_6$O$_7$S$_3$: 936.3 found: 936.2. $E_{1/2}$ (MeCN, V versus [FeCp$_2$]$^{+/0}$): –0.94.

[TMEDA-Ni^{II}(Br)(OH)Fe^{III}].—This complex was prepared by the method described for [TMEDA-Fe^{II}(OTf)(OH)Fe^{III}] using Ni^{II}Br$_2$ (73.5 mg, 0.0896 mmol), TMEDA (12.0 mg, 0.103 mmol), and NMe$_4$[Fe^{II}MST] (73.5 mg, 0.0896 mmol) to produce the desired complex as a crystalline solid in a yield of 47%. Dark orange block crystals of [TMEDA-Ni^{II}(OTf)(OH)Fe^{III}] suitable for X-ray diffraction were grown from a CH$_2$Cl$_2$ solution layered under pentane. UV-vis (CH$_2$Cl$_2$ solution λ_{max}/nm (ε_{max}/M^{-1}cm^{-1})) 275(sh), 285(sh), 387(6200). FTIR (ATR, cm^{-1}, selected bands): 3336(OH), 2973, 2912, 2866, 2361, 1601, 1562, 1465, 1308, 1269, 1130, 1072, 1051, 968, 953, 934, 818, 661. (Nujol, cm^{-1}): 3345(OH). Exact mass calcd for [TMEDA-Ni^{II}(OH)Fe^{III}]$^+$, C$_{39}$H$_{62}$FeNiN$_6$O$_7$S$_3$: 936.3 found: 936.1. $E_{1/2}$ (MeCN, V versus [FeCp$_2$]$^{+/0}$): –0.94.

[(en)$_2$-Fe^{II}(OH)Fe^{III}]OTf. Method A.—This salt was prepared as described for the [TMEDA-Fe^{II}(OTf)(OH)Fe^{III}] using Fe^{II}(OTf)$_2$·2MeCN (39.0 mg, 0.0894 mmol), en (10.8 mg, 0.180 mmol), and NMe$_4$[Fe^{II}MST] (73.1 mg, 0.0892 mmol) to produce the desired salt in crystalline yields of 63–87%. Dark orange needle crystals of [(en)$_2$-Fe^{II}(OH)Fe^{III}]OTf suitable for X-ray diffraction were grown from a THF solution layered under pentane. Elemental analysis calcd. for [(en)$_2$-Fe^{II}(OH)Fe^{III}]OTf·C$_5$H$_{12}$, C$_{43}$H$_{74}$F$_3$Fe$_2$N$_8$O$_{10}$S$_4$: C, 44.52; H, 6.43; N, 9.66%, found: C, 44.84; H, 6.13; N, 9.78%. UV-vis (CH$_2$Cl$_2$, λ_{max}, nm (ε_{max}, M^{-1}cm^{-1})) 274(sh), 283(sh), 339(9500), 382(sh), 524(50.). FTIR (ATR, cm^{-1},

selected bands): 3325(NH), 3268(NH), 3159(NH), 2962, 2934, 2862, 1603, 1449, 1253, 1225, 1153, 1135, 1082, 1028, 968, 939, 822, 797, 656, 637. (Nujol, cm^{-1}): 3235(NH), 3265(NH), 3160(NH). Exact mass calcd for $[(en)_2\text{-}Fe^{III}(O)Fe^{III}]^+$, $C_{37}H_{61}Fe_2N_8O_7S_3$: 937.4 found: 937.3. E_C (MeCN, V versus $[FeCp_2]^{+/0}$): –1.06.

Method B.—A solution of $[TMEDA\text{-}Fe^{II}(OTf)(OH)Fe^{III}]$ (88.0 mg, 0.0812 mmol) in CH_2Cl_2 (10 mL) was treated with en (10.9 mg, 0.0824 mmol) and stirred. After 2 h, the solvent was removed under vacuum and the resulting solid was redissolved in THF. This THF solution was layered under pentane to produce the desired salt with a crystalline yield of 31–39%. This reaction could also be monitored by UV-vis spectroscopy: a 3 mL CH_2Cl_2 solution of $[TMEDA\text{-}Fe^{II}(OTf)(OH)Fe^{III}]$ (0.3 μmol, 0.1 mM) was transferred to a 1.0 cm quartz cuvette under Ar and sealed with a rubber septum. In a spectrophotometer, two equiv. of en (0.6 μmol, 30 mM), prepared under Ar, were injected to the cuvette *via* a gas-tight syringe and the spectral changes monitored every 120 s. The absorbance properties match those obtained for $[(en)_2\text{-}Fe^{II}(OH)Fe^{III}]OTf$ prepared by Method A.

Physical Methods—Elemental analyses were performed on a Perkin-Elmer 2400 CHNS analyzer. UV-visible (UV-vis) spectra were recorded with a Cary 50 spectrophotometer or an Agilent 8453 spectrophotometer equipped with an Unisoku Unispeks cryostat using either a 0.10 cm or 1.00 cm quartz cuvette. FTIR spectra were collected on a Varian 800 Scimitar Series FTIR spectrometer in air or a Thermo Scientific Nicolet iS5 spectrophotometer with an iD5 an attenuated total reflectance (ATR) attachment in a dinitrogen filled glovebox. High-resolution mass spectra were collected using Waters Micromass LCT Premier Mass Spectrometer. CV experiments were conducted using a CH1600C electrochemical analyzer. A 2.0 mm glassy carbon electrode was used as the working electrode at scan velocities 0.1 V s^{-1}. The ferrocenium/ferrocene couple $[FeCp_2]^{+/0}$ was used as an internal reference to monitor the reference electrode ($Ag^{0/+}$). Tetrabutylammonium hexafluorophosphate (TBAP) was use as the supporting electrolyte at a concentration of 0.1 M. Perpendicular-mode X-band EPR spectra were collected using a Bruker EMX spectrometer at 4 K using liquid helium.

Crystallography—A Bruker SMART APEX II diffractometer and the APEX2 program package was used to determine the unit-cell parameters and for data collection. Crystallographic details are summarized in the supporting information, and in Table S1 and S2.

Results and Discussion

Preparation and characterization of the diiron compounds

The preparation of the mixed valent, diiron bimetallic complex $[TMEDA\text{-}Fe^{II}(OTf)(OH)Fe^{III}]$, was achieved *via* the synthetic route outlined in Scheme 1. In a typical reaction, a CH_2Cl_2 or THF suspension of TMEDA, $NMe_4[Fe^{II}MST]$, and $Fe^{II}(OTf)_2{\cdot}2MeCN$ was treated with 0.5 equiv. of O_2 for 1 h. Crystals suitable for X-ray diffraction were obtained by layering a THF solution of $[TMEDA\text{-}Fe^{II}(OTf)(OH)Fe^{III}]$ under pentane, resulting in needle-shaped crystals in yields ranging from 62–87%. If $Fe^{II}Br_2$ was used instead of

$Fe^{II}(OTf)_2$·2MeCN in Scheme 1, [TMEDA-Fe^{II}(Br)(OH)Fe^{III}] was prepared. This result demonstrated that the diiron complexes could be prepared with different types of anionic ligands bound to the Fe^{II} centre, suggesting that other ligands could also bind at the sixth coordination site.

The substitution lability of the triflate ligand was further probed by conducting metathesis reactions with SCN^- or N_3^- ions (Scheme 2). FTIR spectroscopy was used to follow these reactions and revealed that the new [TMEDA-Fe^{II}(X)(OH)Fe^{III}] complexes had characteristic bands for the NCS^- (ν = 2064 cm^{-1}) and N_3^- (ν = 2069 cm^{-1}) ligands (Figure 3B). These bands are at higher energy than the analogous bands of NMe_4(SCN) (2058 cm^{-1})[45] and $NMe_4(N_3)$ (1998 cm^{-1}),[46] suggesting that that these anions are coordinated to the Fe^{II} centre.[46] Additionally, the disappearance of vibrational bands at 1239, 1034, 635 cm^{-1} that are attributed to the that OTf^- ligand supports these substitution reactions.[47] The four diiron compounds otherwise have similar vibrational properties. Each has a ν(OH) band observed around 3200–3300 cm^{-1} (Figure 3A), in which the broadness of these bands suggest the presence of an intramolecular H-bond between the bridging hydroxido ligands and one of the sulfonamido oxygen atoms from $[MST]^{3-}$.[48,49]

The bimetallic formulation of the four crystalline [TMEDA-Fe^{II}(X)(OH)Fe^{III}] complexes was also supported by electrospray ionization mass spectrometry (ESI-MS), in which the m/z of the molecular ion and experimental isotope patterns matched those calculated for $[TMEDA\text{-}Fe^{II}(OH)Fe^{III}]^+$ (Figure S1A). As these complexes only ionize as $[TMEDA\text{-}Fe^{II}(OH)Fe^{III}]^+$, the identity of the X^- ligand could not be determined by positive mode ESI-MS, but elemental analysis could distinguish the various anions and supports our formulations. The compounds all have similar optical properties, as each have a characteristic absorbance band around λ_{max} = 380 nm and an ε_M = 6100–7000 (Figure S2A). The optical properties are similar to those previously reported for the related $[(TMTACN)M^{II}{-}(\mu\text{-}OH){-}Fe^{III}MST]^+$ complexes (M^{II} = Mn^{II}, Fe^{II}, Co^{II}, Ni^{II}, Cu^{II}, Zn^{II}, denoted as $[TMTACN\text{-}M^{II}(OH)Fe^{III}]^+$).[36,37]

Preparation and characterization of [TMEDA-M^{II}(OTf)(OH)Fe^{III}] compounds

Heterobimetallic complexes [TMEDA-M^{II}(OTf)(OH)Fe^{III}] (M^{II} = Co^{II}, Ni^{II}) were prepared in an analogous fashion to [TMEDA-Fe^{II}(OTf)(OH)Fe^{III}] with either $Co^{II}(OTf)_2$·2MeCN or $Ni^{II}(OTf)_2$·5MeCN (Scheme 3) used as the precursor salts.

The heterobimetallic formulation of the two [TMEDA-M^{II}(OTf)(OH)Fe^{III}] compounds is supported by ESI-MS, in which the molecular weight and experimental isotope patterns matched those calculated for $[TMEDA\text{-}M^{II}(OH)Fe^{III}]^+$ (Figure S1B and C). Additionally, the two heterobimetallic complexes had similar optical properties with the series of [TMEDA-Fe^{II}(X)(OH)Fe^{III}] complexes, suggesting that the identity of the divalent metal ion does not greatly affect this property. The UV-vis spectra of the hetereobimetallic compounds showed a characteristic absorption band at λ_{max} = 380 nm (ε_M = 4700 (Co^{II}), 6500 (Ni^{II})) that is similar to those of the diiron compounds (Figure S2B). The heterobimetallic complexes also have vibrational properties similar to the diiron complexes (Figure S3). Both [TMEDA-M^{II}(OTf)(OH)Fe^{III}] complexes have a broad peak associated with the ν(OH) that are observed at 3316 and 3341 cm^{-1} for the Co^{II} and Ni^{II} species, respectively. The trend in

vibrational energies of the O–H bond correlates with the Lewis acidities of the M^{II} ion as gauged by the pK_a values for their corresponding $[M^{II}(H_2O)_x]^{2+}$ complexes.[50] The complex with the most Lewis acidic M^{II} ion, [TMEDA-Fe^{II}(OTf)(OH)Fe^{III}] (pK_a $[Fe^{II}(H_2O)_6]^{2+}$ = 9.5), has the weakest ν(OH) (3271 cm^{-1}) while the one with the least Lewis acidic metal ion, [TMEDA-Ni^{II}(OTf)(OH)Fe^{III}] (pK_a $[Ni^{II}(H_2O)_6]^{2+}$ = 9.9), has the strongest ν(OH) (3341 cm^{-1}).

Solid-state molecular structures of [TMEDA-Fe^{II}(X)(OH)Fe^{III}] compounds.

The molecular structures of the [TMEDA-Fe^{II}(X)(OH)Fe^{III}] complexes were determined by X-ray diffraction methods to reveal their bimetallic structures (Figure 4). Selected metrical parameters and calculated values are shown in Table 1. The five-coordinate Fe^{III} centres contain a N_4O primary coordination sphere formed by the $[MST]^{3-}$ ligand and bridging hydroxido ligand, and adopts a distorted trigonal bipyramidal (tbp) geometry based on the structural parameter τ_5 = 0.854–0.914, where ideal tbp geometry has τ_5 = 1 and ideal square pyramidal geometry has τ_5 = 0.[51] The six-coordinate Fe^{II} centres have a N_3O_2X (X = O (OTf^-), Br (Br^-), N (NCS^- and N_3^-)) primary coordination sphere that adopts a distorted octahedral geometry as evaluated using the octahedral quadratic elongation parameter λ_{oct} = 1.012–1.036, where ideal octahedral geometry has λ_{oct} = 1 and higher values reflect greater distortion from this idealized geometry.[53] The equatorial plane is formed by the sulfonamido O-atoms of $[MST]^{3-}$ (O4, O6) and the N-atoms of the TMEDA ligand (N5, N6). The axial positions are occupied by O-atom of the bridging hydroxido ligand (O1) and the X^- ligand with O1–Fe2–X angles that range from 173.49(5)–175.38(5)˚.

The Fe2–X distances reflect the expected differences in the coordinating atoms in these various ligands. The longest Fe2–X bond is Fe2–Br1 which agrees with the Br^- ion having the largest ionic radius.[54] This long bond causes the greatest octahedral distortion of this series of compounds. The Fe2–X distances for the NCS^- and N_3^- compounds are similar, which consistent with the assignment that the thiocyanate ligand coordinates *via* its N-atom.

The distances between O1···O2 range from 2.611–2.659 Å that indicates intramolecular H-bonds are formed between the H-atom of the hydroxido ligand and O2 of the $[MST]^{3-}$ ligand.[55] These distances are shorter than those reported for the related heterobimetallic complexes $[L\supset M^{II}{-}(\mu\text{-}OH){-}M^{III}MST]^+$, ($L\supset M^{II}$ = 15-crown-5⊃Ca^{II}, 15-crown-5⊃Sr^{II}, or 18-crown-6⊃Ba^{II}, M^{III} = Mn^{III} or Fe^{III}), which have statistically longer O1···O2 distances that range from 2.685–2.700 Å.[35] These distances suggest that the H-bonding is stronger in the diiron complexes, an expect conclusion given our vibrational results and the pK_a values observed for the $[M^{II}(H_2O)_x]^{2+}$ complexes.[48–50]

Solid-state molecular structures of [TMEDA-M^{II}(X)(OH) Fe^{III}] compounds

The molecular structures of the [TMEDA-M^{II}(X)(OH)Fe^{III}] compounds were also determined by X-ray diffraction methods and their structures are shown in Figure 5 with selected metrical parameters presented in Table 2. Because the data for [TMEDA-Ni^{II}(OTf)(OH)Fe^{III}] was not of sufficient quality to obtain an accurate structure (Figure S4), the solid-state structure of the analogous compound [TMEDA-Ni^{II}(Br)(OH)-Fe^{III}] was obtained and used for comparison.

The metrical parameters of the five-coordinate Fe^{III} centre in the two heterobimetallic complexes were similar to those of the diiron compounds and also contain distorted tbp N_4O primary coordination spheres (τ_5 = 0.864–0.892).[51] The six-coordinate M^{II} centres have distorted octahedral geometry with N_3O_2X primary coordination spheres (λ_{oct} = 1.012–1.132)[53] (Figure 5) with the sixth coordination site occupied by either triflate or bromide ligands.

The different ionic radii of the divalent metal ions are reflected most noticeably in the bonds to the TMEDA ligand (that is, the M1–N5 and M1–N6 bonds). The Fe^{II} ion has the greatest radius, and therefore [TMEDA-Fe^{II}(OTf)(OH)Fe^{III}] contains the longest average M1–N_{TMEDA} bonds (2.221 Å). In contrast, [TMEDA-Ni^{II}(OTf)(OH)Fe^{III}] has the shortest average M1–N_{TMEDA} bonds (2.137 Å), reflecting the smaller radius of Ni^{II} ion. These bond lengths are typical of M^{II}–TMEDA complexes, which range between 2.0–2.3 Å.[56–59] A similar observation was found in the related TMTACN complexes, in which the average M^{II}–N_{TMTACN} bond distances decreased with decreasing ionic radii.[54] The placement of the metal ions within [TMEDA-Co^{II}(OTf)(OH)Fe^{III}] are assigned as in the other bimetallic complexes, with the Fe^{III} ion being housed with the N_4 binding site of $[MST]^{3-}$. The metrical parameters around the metal centre in this site are consistent with an Fe^{III} centre and not a Co^{III} ion.[34]

Electrochemical properties of [TMEDA-Fe^{II}(X)(OH)Fe^{III}] and [TMEDA-M^{II}(OTf)(OH)Fe^{III}] compounds

The electrochemical properties of the series of bimetallic complexes were probed using cyclic voltammetry (CV) (Figure S5 and Table 3). All the diiron compounds exhibited a one-electron reductive event that was assigned to the $Fe^{II}Fe^{II}/Fe^{II}Fe^{III}$ couple. In general, the redox potentials of the [TMEDA-Fe^{II}(X)(OH)Fe^{III}] complexes are similar to those of the related TMTACN diiron compound, which has a $Fe^{II}Fe^{II}/Fe^{II}Fe^{III}$ couple at –0.86 V versus $[FeCp_2]^{+/0}$. The voltammograms for the complexes with OTf^-, Br^-, and NCS^- ligands had $Fe^{II}Fe^{II}/Fe^{II}Fe^{III}$ potentials ranging from –0.84 to –0.89 V versus $[FeCp_2]^{+/0}$; however, the voltammogram of the N_3^- complex was irreversible with an E_C = –0.99 V versus $[FeCp_2]^{+/0}$. Slightly lower potentials were observed for the complexes with NCS^- and N_3^- ligands.

An irreversible oxidative process was observed for the four diiron compounds and was assigned to the $Fe^{III}Fe^{III}/Fe^{II}Fe^{III}$ couple. They all occur at similar potentials (+0.82 to 0.84 V versus $[FeCp_2]^{+/0}$) except for that of the NCS^- complex (+0.98 V versus $[FeCp_2]^{+/0}$), and these potentials are all more positive that the analogous potentials reported for the related TMTACN diiron complex (0.35 V versus $[FeCp_2]^{+/0}$). The TMEDA compounds may be harder to oxidize than the TMTACN compounds because the X^- ligands should be poorer ligands than the amine N-atom from TMTACN.

The two heterobimetallic compounds both exhibited a nearly reversible one-electron redox event, which was assigned to the $M^{II}Fe^{II}/M^{II}Fe^{III}$ couple (Figure S5). The $Co^{II}Fe^{III}/Co^{II}Fe^{II}$ redox potential for [TMEDA-Co^{II}(OTf)(OH)Fe^{III}] (–0.86 V versus $[FeCp_2]^{+/0}$) is comparable to other complexes in this series.[37] The potential for the [TMEDA-Ni^{II}(OTf)(OH)Fe^{III}] species (–0.94 V versus $[FeCp_2]^{+/0}$) is more negative by nearly 0.1 V relative to

other complexes in this series: note that a similar type of shift was observed for [TMTACN-Ni^{II}(OH)Fe^{III}]$^{+}$ (–0.99 V versus [$FeCp_2$]$^{+/0}$) when compared to the other complexes in the [TMTACN-M^{II}(OH)Fe^{III}]$^{+}$ series, which all fell within a 0.04 V range.[37] The reason for these shifts for the Ni^{II}-based compounds is unclear.

No additional oxidative features were observable for the heterobimetallic species. The oxidation potentials of Co^{II} and Ni^{II} should be anodically shifted when compared to that of [TMEDA-Fe^{II}(OTf)(OH)Fe^{III}], as late transition metal ions tend to have more positive oxidization potentials, so the $M^{II}Fe^{III}/M^{III}Fe^{III}$ couples were likely too positive to be detected.

Magnetic properties of the [TMEDA-Fe^{II}(X)(OH)Fe^{III}] and [TMEDA-M^{II}(OTf)(OH)Fe^{III}] complexes

The magnetic properties of the [TMEDA-Fe^{II}(X)(OH)Fe^{III}] and [TMEDA-M^{II}(OTf)(OH)Fe^{III}] compounds were probed using X-band EPR spectroscopy. Each complex in the [TMEDA-Fe^{II}(X)(OH)Fe^{III}] series exhibited rhombic perpendicular-mode EPR signals centred around g = 2 (Figure S6A) that are consistent with an $S = 1/2$ spin ground state. This spin state arises from the antiferromagnetic coupling between the high-spin Fe^{III} centre (S = 5/2) and Fe^{II} centre (S = 2). A similar type of coupling and spectrum was observed for the previously reported mixed-valent complex [TMTACN-Fe^{II}(OH)Fe^{III}]$^{+}$.

The heterobimetallic compound [TMEDA-Ni^{II}(OTf)(OH)Fe^{III}] also had EPR properties that are consistent with antiferromagnetic coupling between the two metal centres. An EPR spectrum for this complex was observed that is indicative of an $S = 3/2$ spin ground state (Figure S6B) that is produced from the coupling between the high-spin Fe^{III} centre and the Ni^{II} centre ($S = 1$). For the remaining complex, [TMEDA-Co^{II}(OTf)(OH)Fe^{III}], we were unable to observe EPR signals in either perpendicular- or parallel-modes, which suggests that it has either an $S = 1$ or $S = 2$ spin state. Co^{II} centres often has large spin-orbit coupling that cause the resulting coupled system to have a large D-value that prevents detectable EPR signals at X-band. Again, similar results were observed for analogous heterobimetallic complexes of [TMTACN-M^{II}(OH)Fe^{III}]$^{+}$ (M^{II} = Co^{II}, Ni^{II}). Evans' method[60] was used to determine an effective magnetic moment of 5.8 μ_B for [TMEDA-Co^{II}(OTf)(OH)Fe^{III}] in solution at room temperature. This value is slightly lower than the expected spin-only value of 5.9 μ_B which is suggestive of weak coupling between the metal centres.

Preparation and characterization of [$(en)_2$-Fe^{II}(OH)Fe^{III}] OTf

The ability to modulate the capping ligand on the [TMEDA-M^{II}(X)(OH)Fe^{III}] complexes was also explored. We screened other bidentate capping ligands using the preparative routes outlined in Scheme 1. We found that only en produced a well-defined bimetallic product. A modified procedure was developed to produce this complex in crystalline yields of 63–87%. In a typical reaction, treating [TMEDA-Fe^{II}(OTf)(OH)Fe^{III}] with two equiv. of en (Scheme 4) afford the complex that has the formula [$(en)_2$-Fe^{II}(OH)Fe^{III}]OTf. This process was monitored by UV-vis spectroscopy and showed the clear conversion to the ethylenediamine complex (Figure 6A).

The solid-state molecular structure revealed a discretely bimetallic product that maintains a $Fe^{II}(OH)Fe^{III}$ bimetallic core, but contains two en ligands bonded to the Fe^{II} centre, resulting in a complex with the formulation $[(en)_2\text{-}Fe^{II}(OH)Fe^{III}]OTf$ (Figure 7). Selected metrical parameters and calculated values are shown in Table 4.

The primary coordination sphere of the Fe^{II} centre in $[(en)_2\text{-}Fe^{II}(OH)Fe^{III}]OTf$ is composed of an N_4O_2 donor set with four N-atom donors from the two en ligands, one O-atom donor from the hydroxido ligand, and one O-atom donor from one of the three sulfonamido arms of $[MST]^{3-}$. The remaining two sulfonamido arms form two intramolecular H-bonds: one with the bridging hydroxido ligand (O1···O2 = 2.933(4) Å) and another with a NH group of an en ligands (N6···O4 = 2.832(4) Å).[55] Additionally, a third intermolecular H-bond is observed between the one of the en ligands and the OTf^- counter anion (N5···O8 = 2.982(4) Å). The introduction of the en ligands thus creates a more complicated H-bonding network in $[(en)_2\text{-}Fe^{II}(OH)Fe^{III}]OTf$ than in the other related bimetallic compounds.[37]

The physical properties of $[(en)_2\text{-}Fe^{II}(OH)Fe^{III}]OTf$ were similar to the related $[TMEDA\text{-}Fe^{II}(X)(OH)Fe^{III}]$ compounds. New vibrational bands were observed in the FTIR spectrum of $[(en)_2\text{-}Fe^{II}(OH)Fe^{III}]OTf$ that were close in energy to the NH vibrations of free en, consistent with its formulation (Figure 6B). The rest of the spectrum was similar to those of $[TMEDA\text{-}Fe^{II}(X)(OH)Fe^{III}]$. As found for $[TMEDA\text{-}Fe^{II}(X)(OH)Fe^{III}]$ complexes, the perpendicular-mode EPR spectrum of $[(en)_2\text{-}Fe^{II}(OH)Fe^{III}]OTf$ is consistent with a S = 1/2 spin (Figure S6C). Cyclic voltammetry studies revealed an irreversible one-electron reductive event at –1.1 V versus $[FeCp_2]^{+/0}$ that was assigned to the $Fe^{II}Fe^{II}/Fe^{II}Fe^{III}$ couple, as well as an irreversible one-electron oxidative event at 0.82 V versus $[FeCp_2]^{+/0}$ (Figure S7).

Conclusions

This work has described the preparation and characterization of several new bimetallic complexes prepared with the ligand $[MST]^{3-}$. These mixed valent compounds contain a Fe^{III} centre bound by $[MST]^{3-}$ that is bridged to a second divalent metal centre through a hydroxido ligand. The system is highly modular, as several key components of the system can be altered.

Four diiron compounds, $[TMEDA\text{-}Fe^{II}(X)(OH)Fe^{III}]$, were prepared and studied. Notability, $[TMEDA\text{-}Fe^{II}(OTf)(OH)Fe^{III}]$ contains an OTf^- ligand that is substitutionally labile. This feature was used to prepare isothiocyanate and azide complexes by using $[TMEDA\text{-}Fe^{II}(OTf)(OH)Fe^{III}]$ as a synthon.

Additionally, modifying the initial synthesis of $[TMEDA\text{-}Fe^{II}(OTf)(OH)Fe^{III}]$ with $Fe^{II}Br_2$ allowed for the preparation of $[TMEDA\text{-}Fe^{II}(Br)(OH)Fe^{III}]$. The four diiron compounds all have S = 1/2 perpendicular-mode EPR signals, though the line shapes are different. This may suggest that the X^- ligand remain bound in solution, but this conclusion is disputed by the electrochemical data. The other physical properties of the four diiron compounds are very similar.

In addition to the homobimetallic compounds, the heterobimetallic compounds [TMEDA-Co^{II}(OTf)(OH)Fe^{III}] and [TMEDA-Ni^{II}(OTf)(OH)Fe^{III}] were prepared and characterized. These compounds have similar spectroscopic features to the diiron compounds, but notably vary in their magnetic properties due to the identities of the second divalent metal centre. Moreover, their structural and electrochemical properties rule out that possibility of metal ion scrambling has occurred between the two sites.

Finally, the compound [$(en)_2$-Fe^{II}(OH)Fe^{III}]OTf was prepared by treating [TMEDA-Fe^{II}(OTf)(OH)Fe^{III}] with 2 equiv. of en. The solid-state structure of this complex revealed that two en ligands are bound to the Fe^{II} centre, in contrast to the single capping ligand observed for all other bimetallic complexes prepared with $[MST]^{3-}$. The primary and secondary coordination spheres of [$(en)_2$-Fe^{II}(OH)Fe^{III}]OTf are different from the related diiron compound with TMEDA, as one sulfonamido ligand arm no longer binds to the Fe^{II} centre. Instead, it is involved in H-bonding with one NH groups of the en ligands. This result stresses the importance of the identity of the capping ligand in these types of compounds and emphasizes the high degree of modularity observed in this bimetallic system.

Supplementary Material

Refer to Web version on PubMed Central for supplementary material.

Acknowledgements

We thank the NIH (GM050781) for financial support of this work.

Notes and references

1. McCollum DG, Yap GPA, Liable-Sands L and Rheingold AL, Inorg. Chem, 1997, 36, 2230–2235. [PubMed: 11669851]
2. Incarvito C, Rheingold AL, Gavrilova AL, Qin CJ and Bosnich B, Inorg. Chem, 2001, 40, 4101–4108. [PubMed: 11487311]
3. Shibasaki M and Yamamoto Y, in Multimetallic Catalysts in Organic Synthesis, eds. Shibasaki M and Yamamoto Y, Wiley-VCH, 2004, pp. XI–XII.
4. Powers DC, Benitez D, Tkatchouk E, Goddard WA and Ritter T, J. Am. Chem. Soc, 2010, 132, 14092–14103. [PubMed: 20858006]
5. Shibasaki M, Kanai M, Matsunaga S and Kumagai N, in Bifunctional Molecular Catalysis, Springer Berlin Heidelberg, 2011, pp. 1–30.
6. Mankad NP, Chem. Eur. J, 2016, 22, 5822–5829. [PubMed: 26879884]
7. Ng GKY, Ziller JW and Borovik AS, Inorg. Chem, 2011, 50, 7922–7924. [PubMed: 21793511]
8. Ng GK-Y, Ziller JW and Borovik AS, Chem. Commun, 2012, 48, 2546–8.
9. Kremer AB, Osten KM, Yu I, Ebrahimi T, Aluthge DC and Mehrkhodavandi P, Inorg. Chem, 2016, 55, 5365–5374. [PubMed: 27187767]
10. Buchler S, Meyer F, Kaifer E and Pritzkow H, Inorganica Chim. Acta, 2002, 337, 371–386.
11. Isaac JA, Gennarini F, López I, Thibon-Pourret A, David R, Gellon G, Gennaro B, Philouze C, Meyer F, Demeshko S, Le Mest Y, Réglier M, Jamet H, Le Poul N and Belle C, Inorg. Chem, 2016, 55, 8263–8266. [PubMed: 27518211]
12. Dunn TJ, Ramogida CF, Simmonds C, Paterson A, Wong EWY, Chiang L, Shimazaki Y and Storr T, Inorg. Chem, 2011, 50, 6746–6755. [PubMed: 21675708]
13. Clarke RM, Hazin K, Thompson JR, Savard D, Prosser KE and Storr T, Inorg. Chem, 2016, 55, 762–774. [PubMed: 26719989]

14. Alliger GE, Müller, L. H P Cummins Do, C. C. and Nocera DG, Inorg. Chem, 2011, 50, 4107–4115. [PubMed: 21446665]
15. Borovik AS, Que L, Papaefthymiou V, Münck E, Taylor LF and Anderson OP, J. Am. Chem. Soc, 1988, 110, 1986–1988.
16. Borovik AS, Papaefthymiou V, Taylor LF, Anderson OP and Que L, Jr., J. Am. Chem. Soc, 1989, 111, 6183–6195.
17. Blusch LK, Mitevski O, Martin-Diaconescu V, Pröpper K, DeBeer S, Dechert S and Meyer F, Inorg. Chem, 2014, 53, 7876–7885. [PubMed: 25014112]
18. Rudd PA, Liu S, Gagliardi L, Young VG and Lu CC, J. Am. Chem. Soc, 2011, 133, 20724–20727. [PubMed: 22122804]
19. Clouston LJ, Siedschlag RB, Rudd PA, Planas N, Hu S, Miller AD, Gagliardi L and Lu CC, J. Am. Chem. Soc, 2013, 135, 13142–13148. [PubMed: 23901938]
20. Eisenhart RJ, Clouston LJ and Lu CC, Acc. Chem. Res, 2015, 48, 2885–2894. [PubMed: 26492331]
21. Greenwood BP, Forman SI, Rowe GT, Chen C-H, Foxman BM and Thomas CM, Inorg. Chem, 2009, 48, 6251–6260. [PubMed: 19499941]
22. Krogman JP and Thomas CM, Chem. Commun, 2014, 50, 5115.
23. Wu B, Wilding MJT, Kuppuswamy S, Bezpalko MW, Foxman BM and Thomas CM, Inorg. Chem, 2016, 55, 12137–12148. [PubMed: 27571456]
24. Serrano-Plana J, Garcia-Bosch I, Company A and Costas M, Acc. Chem. Res, 2015, 48, 2397–2406. [PubMed: 26207342]
25. Das B, Daver H, Singh A, Singh R, Haukka M, Demeshko S, Meyer F, Lisensky G, Jarenmark M, Himo F and Nordlander E, Eur. J. Inorg. Chem, 2014, 2014, 2204–2212.
26. Delgado M, Ziegler JM, Seda T, Zakharov LN and Gilbertson JD, Inorg. Chem, 2016, 55, 555–557. [PubMed: 26692111]
27. Lawrence JD, Li H, Rauchfuss TB, Bénard M and Rohmer M-M, Angew. Chemie, 2001, 113, 1818–1821.
28. Barton BE and Rauchfuss TB, J. Am. Chem. Soc, 2010, 132, 14877–14885. [PubMed: 20925337]
29. Li Y and Rauchfuss TB, Chem. Rev, 2016, 116, 7043–7077. [PubMed: 27258046]
30. Evans WJ, Lee DS and Ziller JW, , DOI:10.1021/JA036923M.
31. Evans WJ, Kozimor SA and Ziller JW, Polyhedron, 2006, 25, 484–492.
32. Wong JL, Higgins RF, Bhowmick I, Cao DX, Szigethy G, Ziller JW, Shores MP, Heyduk AF, Gagliardi L and Lu CC, Chem. Sci, 2016, 7, 1594–1599. [PubMed: 28808535]
33. Rosenkoetter KE, Ziller JW and Heyduk AF, Inorg. Chem, 2016, 55, 6794–6798. [PubMed: 27300501]
34. Lacy DC, Park YJ, Ziller JW, Yano J and Borovik AS, J. Am. Chem. Soc, 2012, 134, 17526–17535. [PubMed: 22998407]
35. Park YJ, Cook SA, Sickerman NS, Sano Y, Ziller JW and Borovik AS, Chem. Sci, 2013, 4, 717–726. [PubMed: 24058726]
36. Sano Y, Weitz AC, Ziller JW, Hendrich MP and Borovik AS, Inorg. Chem, 2013, 52, 10229–10231. [PubMed: 23992041]
37. Sano Y, Lau N, Weitz AC, Ziller JW, Hendrich MP and Borovik AS, Inorg. Chem, 2017, 56, 14118–14128. [PubMed: 29112385]
38. Sickerman NS, Henry RM, Ziller JW and Borovik AS, Polyhedron, 2013, 58, 65–70. [PubMed: 25309019]
39. Sickerman NS, Peterson SM, Ziller JW, Borovik AS, Mäemets V, Leito I, Koppel IA and Borovik AS, Chem. Commun, 2014, 50, 2515.
40. Cook SA, Ziller JW and Borovik AS, Inorg. Chem, 2014, 53, 11029–11035. [PubMed: 25264932]
41. Lau N, Ziller JW and Borovik AS, Polyhedron, 2015, 85, 777–782. [PubMed: 25419035]
42. Lau N, Sano Y, Ziller JW and Borovik AS, Polyhedron, 2017, 125, 179–185. [PubMed: 29170577]
43. Park YJ, Ziller JW and Borovik AS, J. Am. Chem. Soc, 2011, 133, 9258–9261. [PubMed: 21595481]

44. Heintz KR, Smith RA, Szalay JA, Weisgerber PS, Dunbar A, Inorg. Synth, 2002, 33, 75–83.
45. Shurdha E, Moore CE, Rheingold AL, Lapidus SH, Stephens PW, Arif AM and Miller JS, Inorg. Chem, 2013, 52, 10583–10594. [PubMed: 23981238]
46. Christe KO, Wilson WW, Bau R and Bunte SW, J. Am. Chem. Soc, 1992, 114, 3411–3414.
47. Johnston DH and Shriver DF, Inorg. Chem, 1993, 32, 1045–1047.
48. Gellman SH, Dado GP, Liang GB and Adams BR, J. Am. Chem. Soc, 1991, 113, 1164–1173.
49. Aaron HS, in Topics in Stereochemistry, Volume 11, eds. Allinger NL and Eliel EL, John Wiley & Sons, Inc., Hoboken, NJ, USA, 1979.
50. Jackson VE, Felmy AR and Dixon DA, J. Phys. Chem. A, 2015, 119, 2926–2939. [PubMed: 25721568]
51. Addison AW, Rao TN, Reedijk J, van Rijn J and Verschoor GC, J. Chem. Soc. Dalt. Trans, 1984, 1349.
52. Balić Žunić T, Vicković I and IUCr J Appl. Crystallogr, 1996, 29, 305–306.
53. Robinson K, Gibbs GV and Ribbe PH, Science, 1971, 172, 567–570. [PubMed: 17802221]
54. Shannon RD, Acta Crystallogr. Sect. A, 1976, 32, 751–767.
55. Emsley J, Chem. Soc. Rev, 1980, 9, 91.
56. Yoshida T, Suzuki T, Kanamori K and Kaizaki S, Inorg. Chem, 1999, 38, 1059–1068. [PubMed: 11670886]
57. Handley DA, Hitchcock PB and Leigh GJ, Inorganica Chim. Acta, 2001, 314, 1–13.
58. Amarasinghe KKD, Chowdhury SK, Heeg MJ and Montgomery J, Organometallics, 2001, 20, 370–372.
59. Madhu V, Bolligarla R, Naik IK, Mekala R and Das SK, Eur. J. Inorg. Chem, 2016, 2016, 4257–4264.
60. Evans DF, J. Chem. Soc, 1959, 2003–2005.

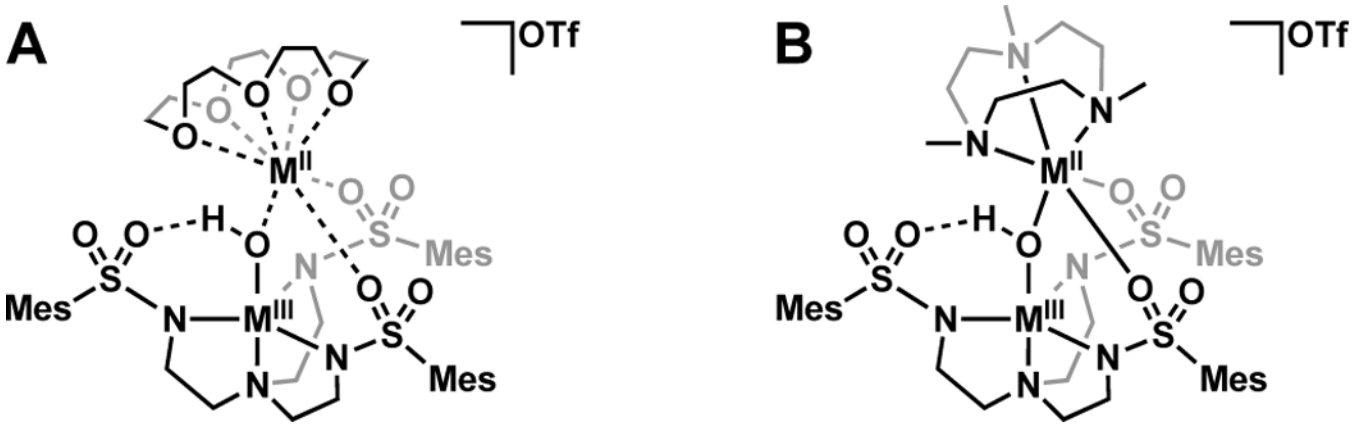

Figure 1.

Specific examples of $[MST]^{3-}$ bimetallic complexes with (**A**) one transition metal ion (M^{III} = Mn^{III}, Fe^{III}) and one redox inactive metal ion (M^{II} = Ca^{II}, Sr^{II}, Ba^{II} (with 18-crown-6))[35] and (**B**) two transition metal ions (M^{III} = Fe^{III}, M^{II} = Mn^{II}, Fe^{II}, Co^{II}, Ni^{II}, Cu^{II}, Zn^{II}).[36,37]

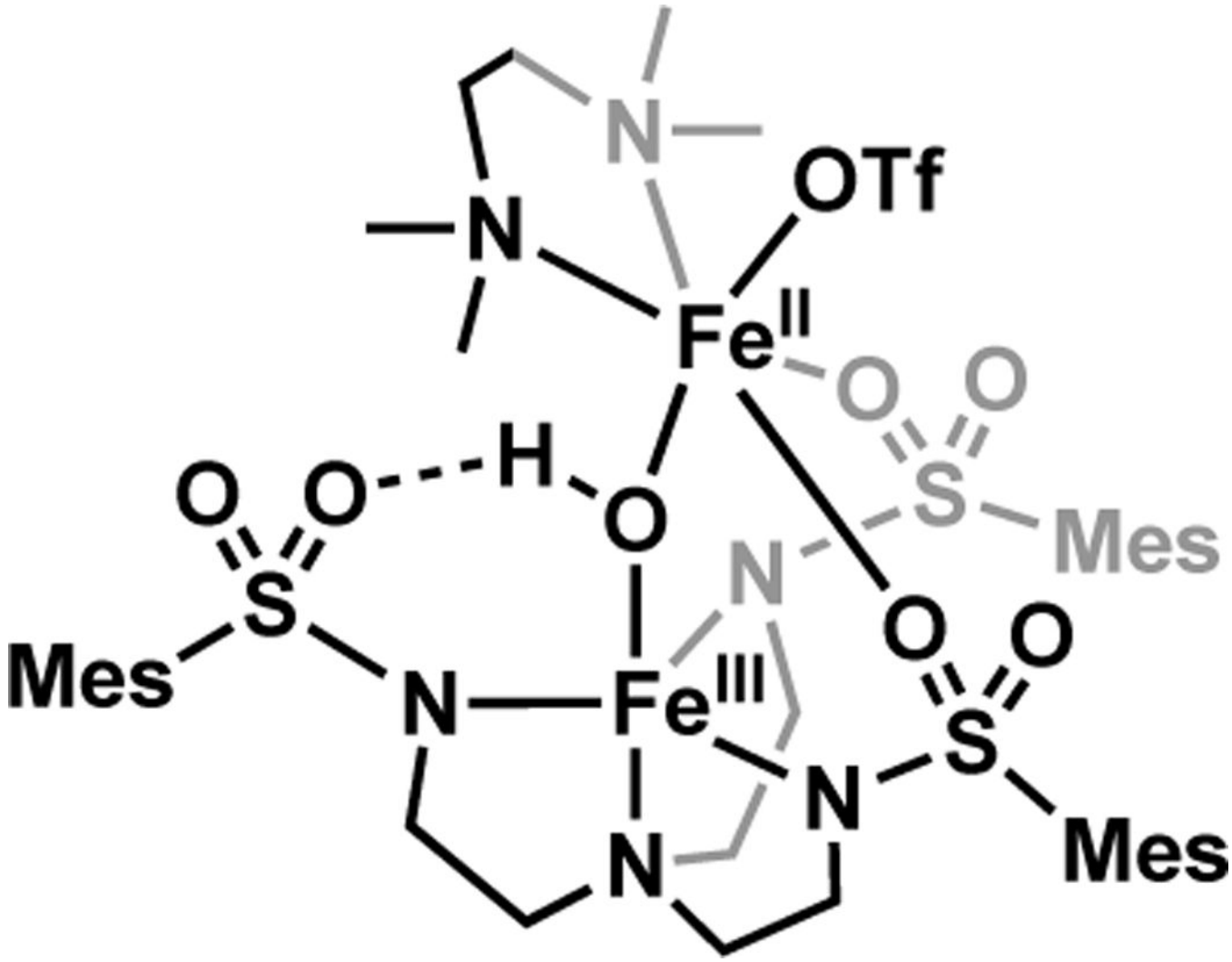

Figure 2.
The new diiron complex prepared with L = TMEDA, [TMEDA-Fe^{II}(OTf)(OH)Fe^{III}].

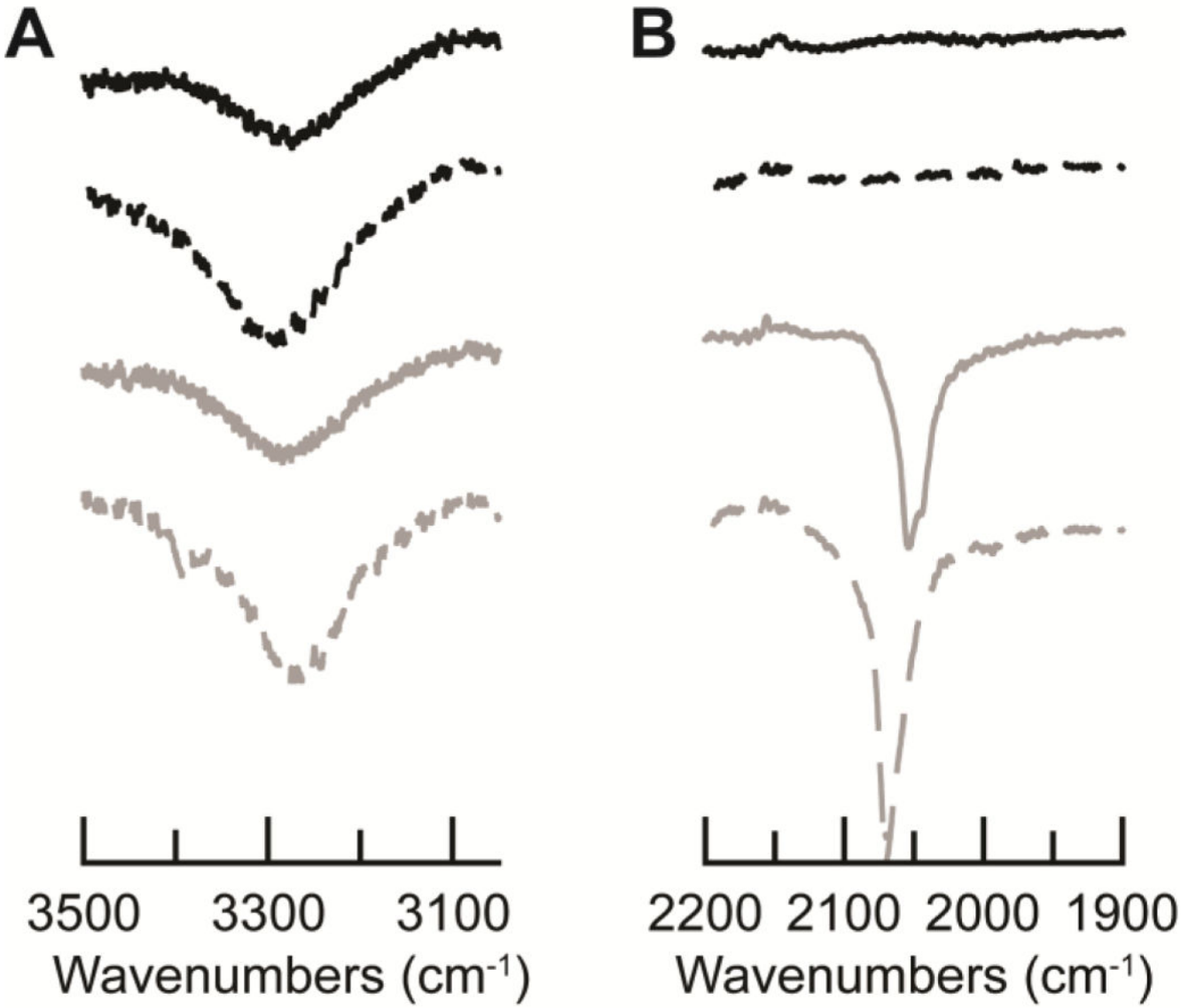

Figure 3.

FTIR spectra of [TMEDA-Fe^{II}(OTf)(OH)Fe^{III}] (solid black), [TMEDA-Fe^{II}(Br)(OH)Fe^{III}] (dashed black), [TMEDA-Fe^{II}(NCS)(OH)Fe^{III}] (solid grey), and [TMEDA-Fe^{II}(OTf)(OH)Fe^{III}] (dashed grey), showing (**A**) the expanded region around ν(OH), (**B**) the region around ν(SCN) and ν(N_3). All spectra were collected by ATR.

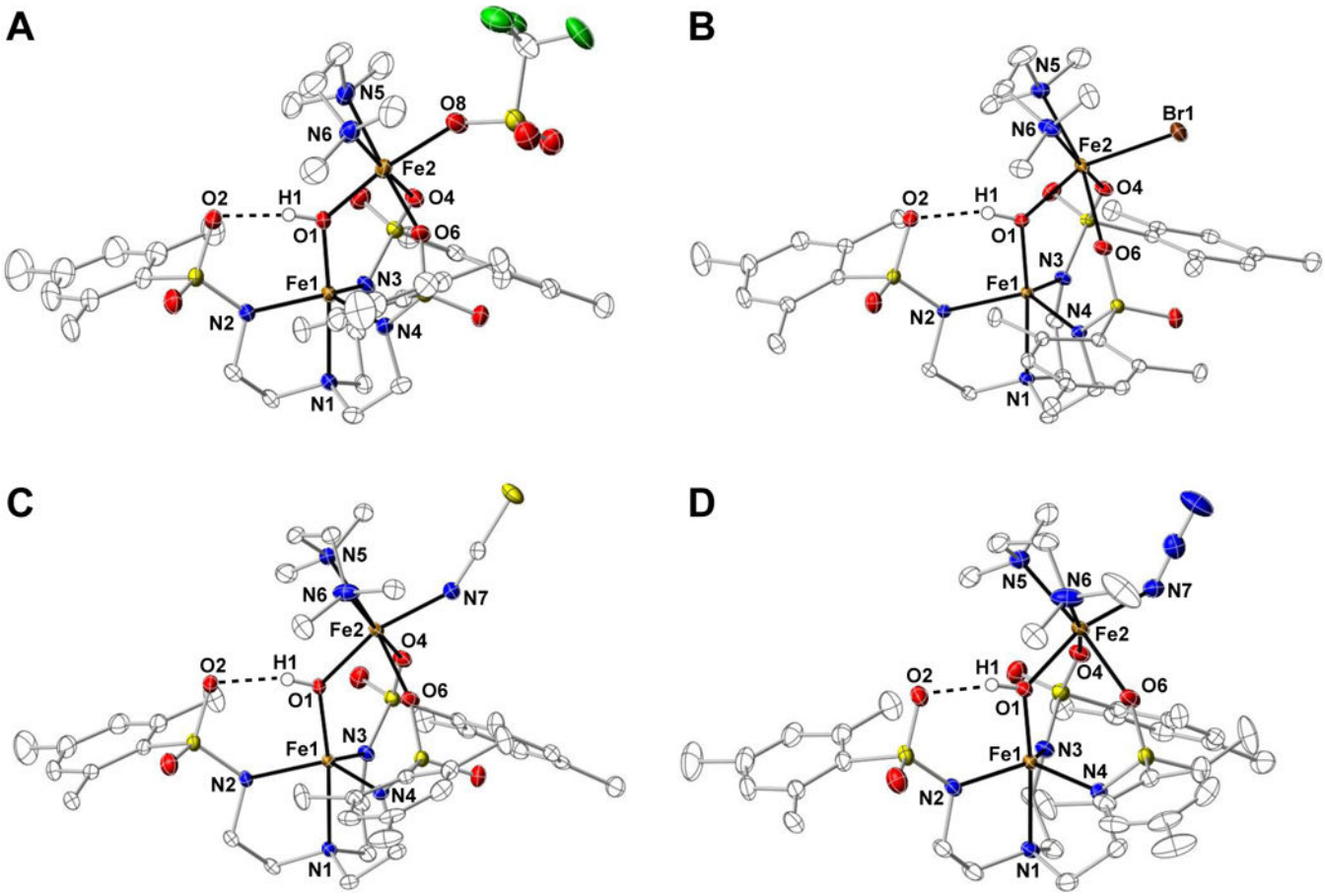

Figure 4.

Thermal ellipsoid diagrams depicting the molecular structures of (**A**) [TMEDA-Fe^{II}(OTf)(OH)Fe^{III}], (**B**) [TMEDA-Fe^{II}(Br)(OH)Fe^{III}], (**C**) [TMEDA-Fe^{II}(NCS)(OH)Fe^{III}], and (**D**) [TMEDA-Fe^{II}(N_3)(OH)Fe^{III}]. Ellipsoids are drawn at the 50% probability level, and only the hydroxido H-atoms are shown for clarity.

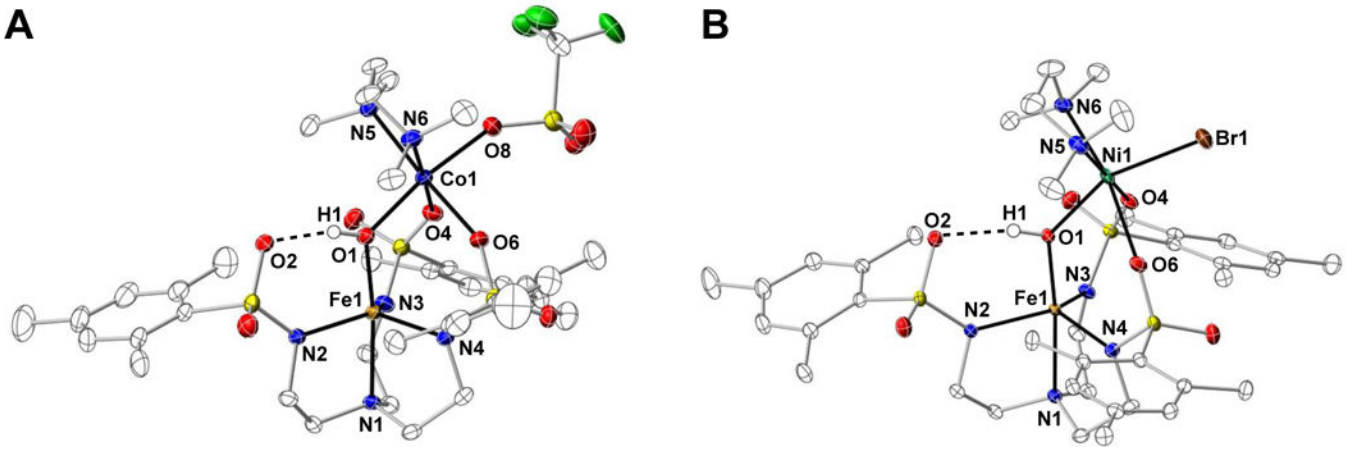

Figure 5.

Thermal ellipsoid diagrams depicting the molecular structures of (**A**) [TMEDA-Co^{II}(OTf)(OH)Fe^{III}] and (**B**) [TMEDA-Ni^{II}(Br)(OH)Fe^{III}]. Ellipsoids are drawn at the 50% probability level, and only the hydroxido H-atoms are shown for clarity.

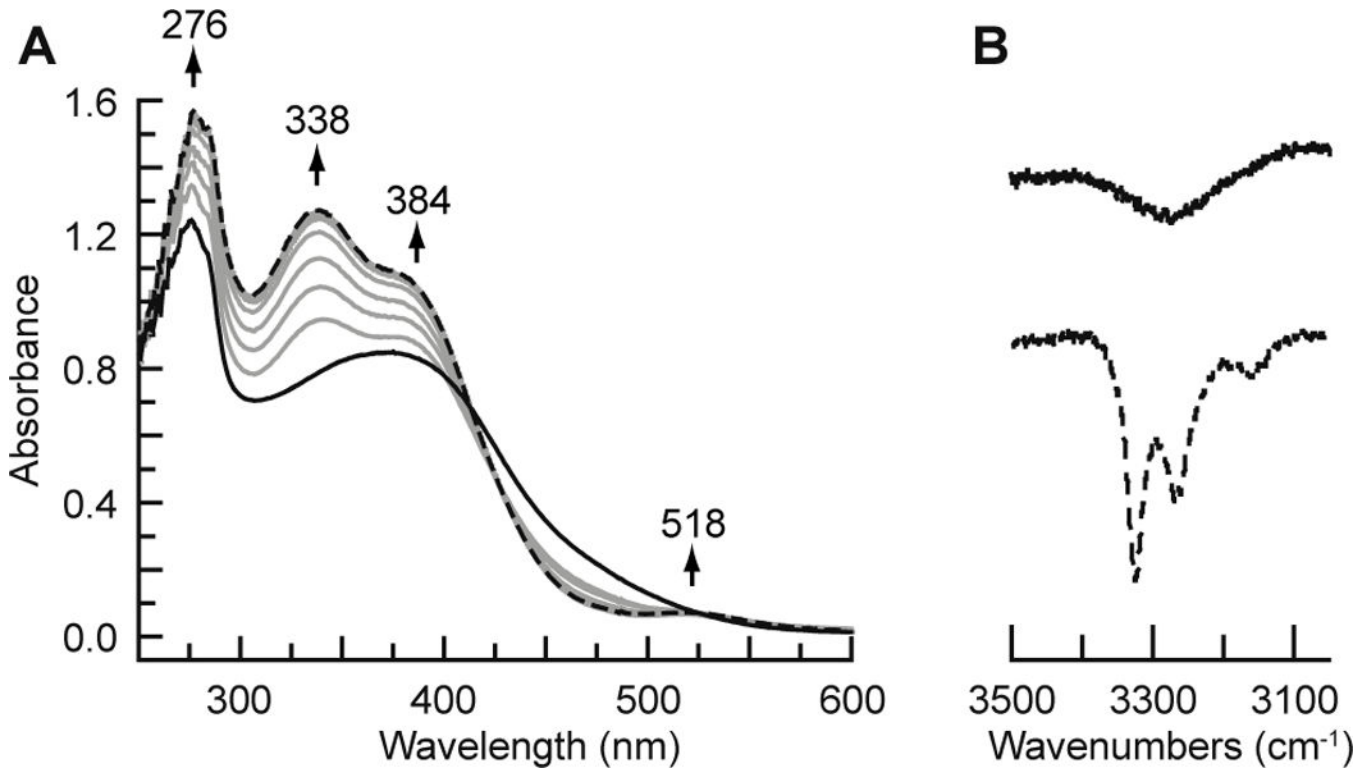

Figure 6.

(**A**) UV-vis spectra for the substitution of TMEDA for en in a 0.1 mM CH_2Cl_2 solution of [TMEDA-Fe^{II}(OTf)(OH)Fe^{III}] at 25 ˚C, showing the conversion of [TMEDA-Fe^{II}(OTf)(OH)Fe^{III}] (solid black) to [$(en)_2$-Fe^{II}(OH)Fe^{III}]OTf (dashed black) after 42 min. (**B**) FTIR spectra of [TMEDA-Fe^{II}(OTf)(OH)Fe^{III}] (solid black) and [$(en)_2$-Fe^{II}(OH)Fe^{III}]OTf (solid black), showing the expanded region around ν(OH) collected by ATR.

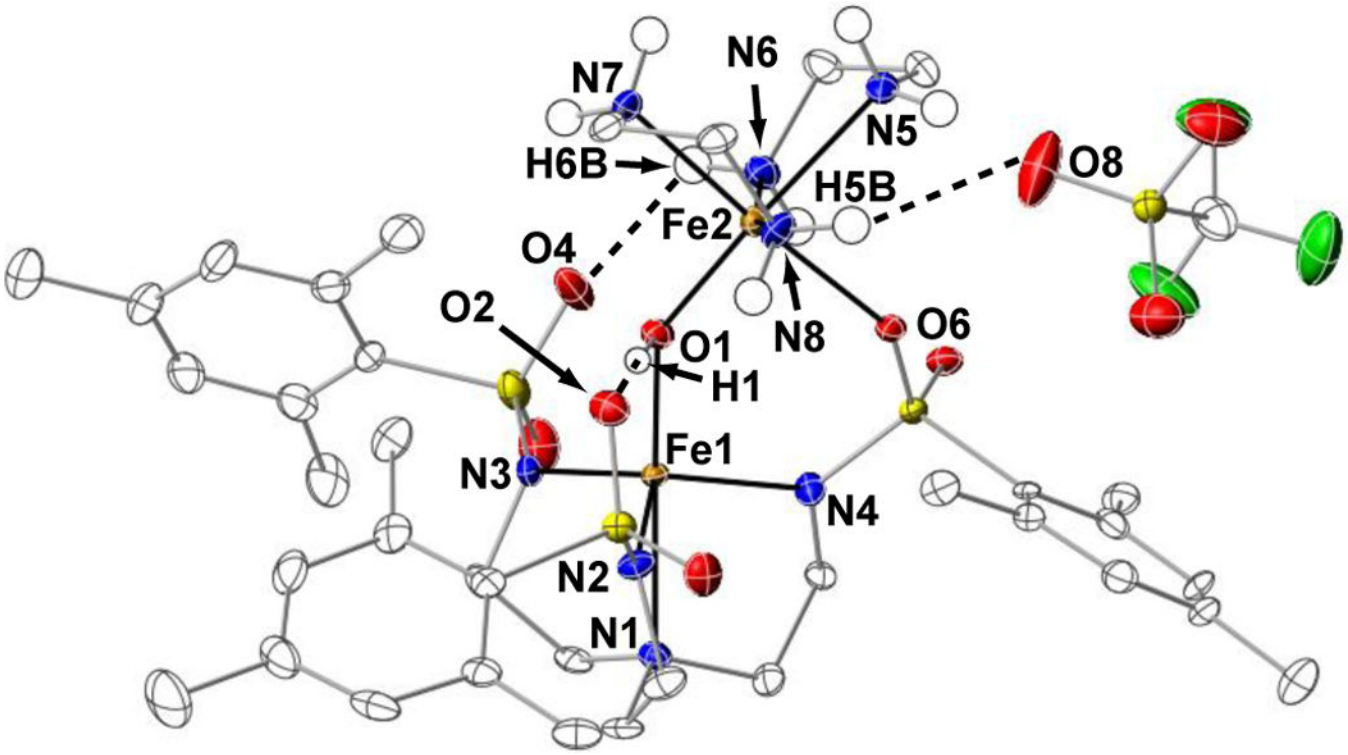

Figure 7.

Thermal ellipsoid diagram depicting the molecular structure of $[(en)_2\text{-}Fe^{II}(OH)Fe^{III}]OTf$. Ellipsoids are drawn at the 50% probability level, and only the hydroxido and en H atoms are shown for clarity.

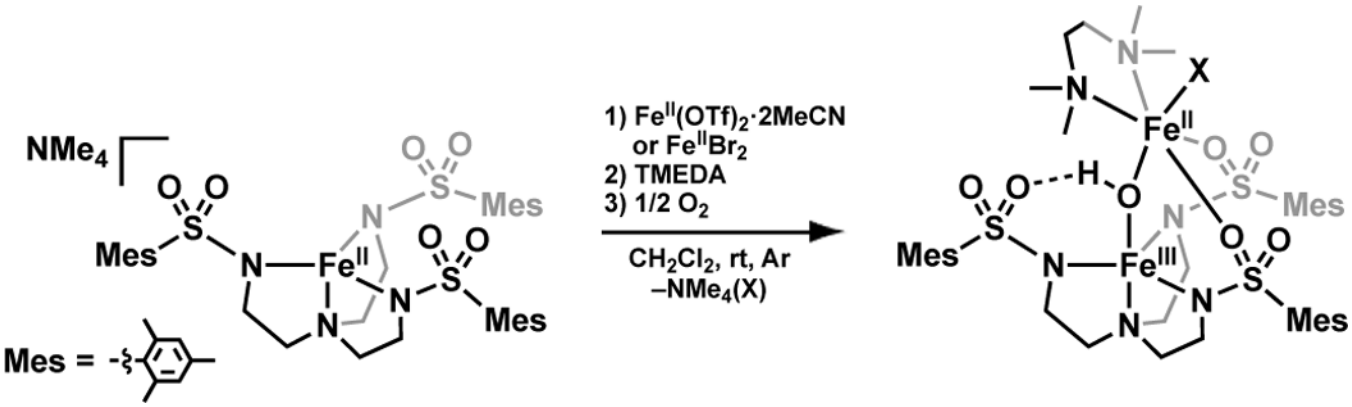

Scheme 1.

Preparation of [TMEDA-Fe^{II}(X)(OH)Fe^{III}] complexes (X^- = OTf^-, Br^-).

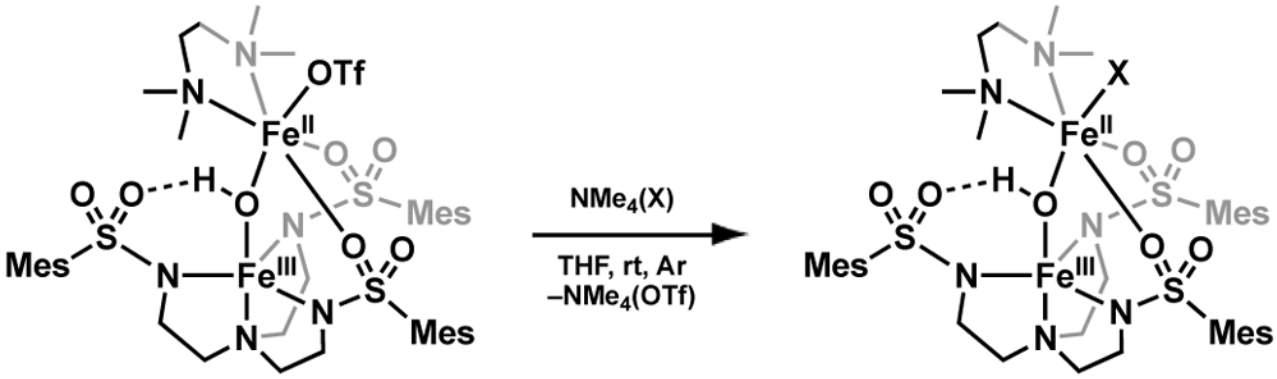

Scheme 2.

Preparation of [TMEDA-Fe^{II}(X)(OH)Fe^{III}] complexes (X^- = NCS^-, N_3^-) *via* metathesis with $NMe_4(X)$ salts.

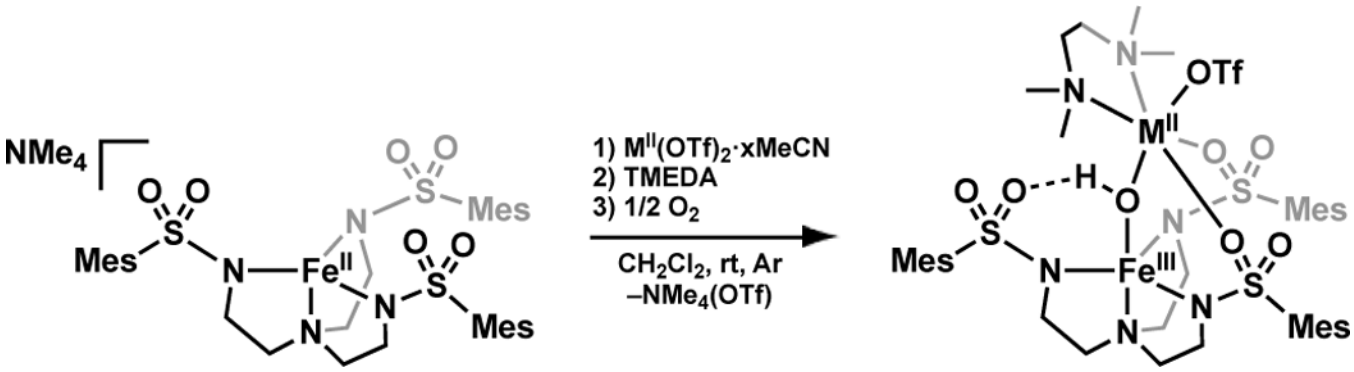

Scheme 3.
Preparation of [TMEDA-M^{II}(OTf)(OH)Fe^{III}] complexes (M^{II} = Co^{II} (x = 2), Ni^{II} (x = 5)).

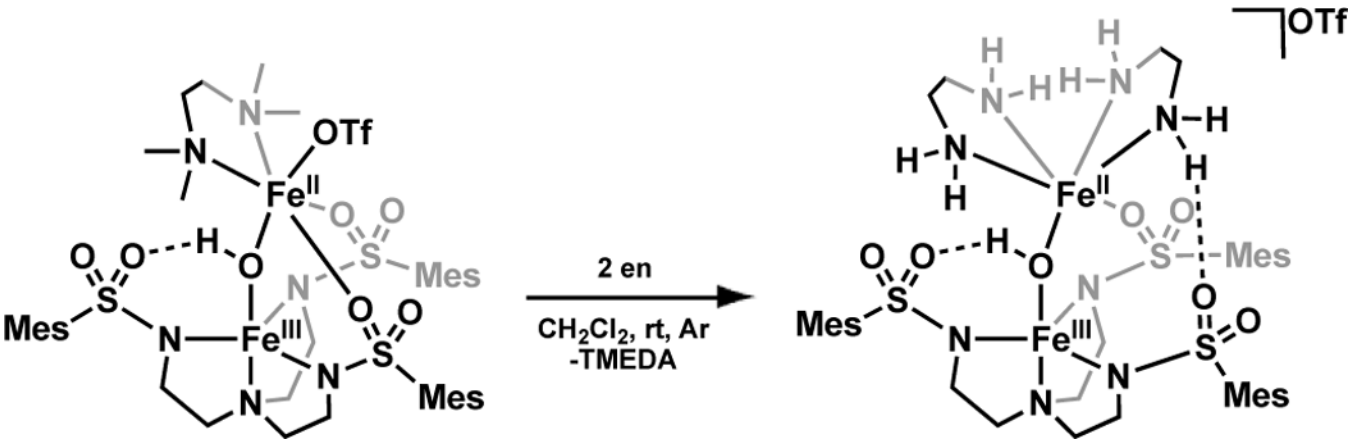

Scheme 4.
Preparation of $[(en)_2\text{-}Fe^{II}(OH)Fe^{III}]OTf$ from $[TMEDA\text{-}Fe^{II}(OTf)(OH)Fe^{III}]$.

Table 1.

Selected metrical parameters for [TMEDA-Fe^{II}(X)(OH)Fe^{III}] (X^- = OTf^-, Br^-, NCS^-, N_3^-) complexes.

[TMEDA-Fe^{II}(X)(OH)Fe^{III}]	X^-			
	OTf^- (O8)	**Br^- (Br1)**	**NCS^-(N7)**	**N_3^- (N7)**
Bond distances (Å)				
Fe1–N1	2.227(2)	2.251(1)	2.220(1)	2.232(2)
Fe1–N2	2.031(2)	2.043(1)	2.032(1)	2.030(2)
Fe1–N3	2.001(2)	1.997(1)	1.997(1)	2.017(2)
Fe1–N4	2.005(2)	2.003(1)	2.016(1)	1.994(2)
Fe1–O1	1.855(2)	1.888(1)	1.886(1)	1.887(2)
O1···O2	2.659(2)	2.658(1)	2.611(1)	2.617(2)
Fe2–O1	1.928(2)	1.983(1)	1.962(1)	1.983(2)
Fe2–O4	2.207(2)	2.276(1)	2.402(1)	2.293(2)
Fe2–O6	2.147(2)	2.499(1)	2.283(1)	2.404(2)
Fe2–N5	2.211(2)	2.263(2)	2.277(2)	2.236(2)
Fe2–N6	2.231(2)	2.238(2)	2.236(2)	2.262(2)
Fe2–O8	2.086(2	–	–	–
Fe2–Br1	–	2.479(3)	–	–
Fe2–N7	–	–	2.040(2)	2.058(2)
Fe1···Fe2	3.337	3.482	3.458	3.482
Avg. Fe1–$N_{eq\text{-}MST}$	2.012	2.014	2.015	2.013
Avg. Fe2–N_{TMEDA}	2.221	2.251	2.257	2.249
d[Fe1–$N_{eq\text{-}MST}$]	0.357	0.387	0.363	0.371
Bond angles (°)				
O1–Fe1–N1	175.20(8)	175.38(5)	173.49(5)	174.72(7)
N2–Fe1–N3	121.10(9)	117.31(6)	117.74(6)	121.29(8)
N2–Fe1–N4	121.72(9)	120.49(6)	122.27(6)	117.55(7)
N3–Fe1–N4	107.86(8)	111.35(6)	110.40(6)	111.18(8)
Fe1–O1–Fe2	126.40(9)	128.09(7)	127.94(7)	128.24(8)
O1–Fe2–O8	171.04(8)	–	–	–
O1–Fe2–Br1	–	157.19(4)	–	–
O1–Fe2–N7	–	–	160.78(6)	158.44(7)
O4–Fe2–O6	96.13(7)	108.73(4)	103.07(4)	104.32(6)
N5–Fe2–N6	82.76(9)	81.53(6)	81.48(6)	81.31(8)
Calculated values				
τ_5 [a]	0.891	0.914	0.854	0.891
V_{oct} [b]	12.8	15.3	13.7	13.7
λ_{oct} [c]	1.012	1.036	1.029	1.034

[a] trigonality parameter, $\tau_5 = (\beta - \alpha)/60$. β is the largest bond angle observed, and α is the second largest bond angle.[51]

[b] octahedral volume, calculated using the IVTON program.[52]

[c] mean oct quadratic elongation, $\lambda_{oct} = \Sigma_1^6(l_i/l_0)^2/6$. $\lambda_{oct} = 1$ for an ideal octahedron. l_0 represents the centre-to-vertex distance of an octahedron with O_h symmetry whose volume is equal to that of the distorted octahedron with distances l_i. λ'_{oct} is the oct quadratic elongation toward one axis.[53]

Table 2.

Selected metrical parameters for [TMEDA-M^{II}(OTf)Fe^{III}] (M^{II} = Co^{II} or Ni^{II}) complexes.

[TMEDA-M^{II}(X)(OH)Fe^{III}]	M^{II} (M1)	
	Co^{II} (Co1)	Ni^{II} (Ni1)
Bond distances (Å)		
Fe1–N1	2.221(2)	2.258(2)
Fe1–N2	2.035(2)	2.049(2)
Fe1–N3	1.992(2)	1.995(2)
Fe1–N4	1.994(2)	1.998(2)
Fe1–O1	1.879(2)	1.893(1)
O1···O2	2.619(2)	2.673(3)
M1–O1	1.971(2)	1.987(1)
M1–O4	2.217(2)	2.172(1)
M1–O6	2.153(2)	2.620(1)
M1–N5	2.194(2)	2.129(2)
M1–N6	2.216(2)	2.144(2)
M1–O8	2.067(2)	–
M1–Br1	–	2.451(3)
Fe1···M1	3.419(2)	3.498(3)
Avg. Fe1–$N_{eq\text{-}MST}$	2.007	2.014
Avg. M1–N_{TMEDA}	2.205	2.137
d[Fe1–$N_{eq\text{-}MST}$]	0.351	0.393
Bond angles (°)		
O1–Fe1–N1	173.62(7)	174.09(6)
N2–Fe1–N3	120.67(8)	117.40(6)
N2–Fe1–N4	121.80(8)	120.55(6)
N3–Fe1–N4	108.48(8)	110.87(7)
Fe1–O1–M1	125.23(9)	128.72(7)
O1–M1–O8	170.23(7)	–
O1–M1–Br1	–	156.12(4)
O4–M1–O6	92.94(6)	103.61(5)
N5–M1–N6	82.90(8)	85.23(7)
Calculated values		
τ_5[a]	0.864	0.892
V_{oct}[b]	12.8	14.6
λ_{oct}[c]	1.012	1.132

Table 3.

Electrochemical data for the [TMEDA-M^{II}(X)(OH)Fe^{III}] complexes in MeCN.[a]

M^{II}	X	$E^{1/2}$($M^{II}Fe^{III}/M^{II}Fe^{II}$, V	E_A($M^{II}Fe^{III}/M^{III}Fe^{III}$, V versus $[FeCp_2]^{+/0}$)
Fe^{II}	OTf^-	–0.84	0.82
Fe^{II}	Br^-	–0.84	0.84
Fe^{II}	NCS^-	–0.89	0.98
Fe^{II}	N_3^-	–0.99[b]	0.84
Co^{II}	OTf^-	–0.86	–
Ni^{II}	OTf^-	–0.94	–

[a] versus $[FeCp_2]^{+/0}$);

[b] EC

Table 4.

Selected metrical parameters for $[(en)_2\text{-}Fe^{II}(OH)Fe^{III}]OTf$.

$[(en)_2\text{-}Fe^{II}(OH)Fe^{III}]OTf$	
Bond distances (Å)	
Fe1–N1	2.334(4)
Fe1–N2	2.030(4)
Fe1–N3	2.017(4)
Fe1–N4	2.044(4)
Fe1–O1	1.792(4)
O1···O2	2.933(4)
Fe2–O1	1.809(4)
Fe2···O4	3.796(4)
Fe2–O6	2.117(4)
Fe2–N5	2.232(4)
Fe2–N6	2.168(4)
Fe2–N7	2.169(4)
Fe2–N8	2.158(4)
Fe1···Fe2	3.366(4)
Avg. $Fe1–N_{eq\text{-}MST}$	2.030(4)
Avg. $Fe2–N_{en}$	2.182(4)
$d[Fe1–N_{eq\text{-}MST}]^a$	0.424
Bond angles (°)	
O1–Fe1–N1	177.23(2)
N2–Fe1–N3	118.46(2)
N2–Fe1–N4	112.05(2)
N3–Fe1–N4	116.77(2)
Fe1–O1–Fe2	138.40(2)
O1–Fe2–O6	92.30(2)
N5–Fe2–N6	77.92(2)
N7–Fe2–N8	81.59(2)
Calculated values	
$\tau_5{}^b$	0.9795
$V_{oct}{}^c$	12.3
$\lambda_{oct}{}^d$	1.015